Mon. Not. R. Astron. Soc. **000**, 000–000 (0000) Printed 10 October 2012 (MN LATEX style file v2.2)

arXiv:1210.2480v1 [astro-ph.CO] 9 Oct 2012

Constraining the substructure of dark matter haloes with galaxy-galaxy lensing

Ran Li[1]*, H.J. Mo[2], Zuhui Fan[3], Xiaohu Yang[4], Frank C. van den Bosch[5]
[1] *National Astronomy Observatory, Chinese Academy of Sciences, Beijing 100871, China*
[2] *Department of Astronomy, University of Massachusetts, Amherst MA 01003, USA*
[3] *Department of Astronomy, Peking University, Beijing 100871, China*
[4] *Shanghai Astronomical Observatory, the Partner Group of MPA, Nandan Road 80, Shanghai 200030, China*
[5] *Astronomy Department, Yale University, P.O. Box 208101 New Haven, CT 06520-8101, USA*

10 October 2012

ABSTRACT
With galaxy groups constructed from the Sloan Digital Sky Survey (SDSS), we analyze the expected galaxy-galaxy lensing signals around satellite galaxies residing in different host haloes and located at different halo-centric distances. We use Markov Chain Monte Carlo (MCMC) method to explore the potential constraints on the mass and density profile of subhaloes associated with satellite galaxies from SDSS-like surveys and surveys similar to the Large Synoptic Survey Telescope (LSST). Our results show that for SDSS-like surveys, we can only set a loose constraint on the mean mass of subhaloes. With LSST-like surveys, however, both the mean mass and the density profile of subhaloes can be well constrained.

Key words: cosmology: dark matter - galaxies: haloes - methods: statistical - galaxies: subhalo - gravitational lensing

1 INTRODUCTION

In the cold dark matter (CDM) scenario, large-scale structures in the universe grow hierarchically through gravitational instabilities. Galaxies are assumed to form in dark matter potential wells through gas cooling and star formation (White & Rees 1978; White & Frenk 1991). During the hierarchical formation process, when small haloes merge into larger systems, they become subhaloes. High resolution simulations show that while some of them are disrupted dure to processes such as tidal stripping and impulsive heating, a large fraction of the subhaloes survive. Hence, probing the masses and density profiles of the population of subhaloes is a key test for the CDM structure formation model.

The mass function, spatial distribution and density profile of subhaloes has been extensively studied with semi-analytical models as well as N-body simulations (e.g., Hayashi et al. 2003; Gao et al. 2004; van den Bosch et al. 2005; Giocoli et al. 2008, 2010; Springel et al. 2008; Zentner & Bullock 2003; Taylor & Babul 2004; Oguri & Lee 2004; Gill et al. 2004) State-of-the-art, high-resolution simulations (Springel et al. 2008; Diemand et al. 2007) can resolve subhaloes down to a mass of $\sim 10^7 \mathrm{h}^{-1}\mathrm{M}_\odot$, and thus provide detailed predictions for both their mass function and density profiles.

On the other hand, it is very challenging to probe dark matter subhaloes observationally because of their darkness and the relatively weak gravitational potential compared to that of their host haloes. Arguably the best (and most direct) probe of dark matter substructure is gravitational lensing. The existence of substructure in a smooth dark matter halo induces flux-ratio anomalies for multiple images of a lensed system (Mao & Schneider 1998; Metcalf & Madau 2001; Mao et al. 2004; Kochanek & Dalal 2004; Macciò & Miranda 2006; Xu et al. 2009), and also perturbs the surface brightness of extended Einstein rings and arcs (Koopmans 2005; Vegetti & Koopmans 2009a,b; Vegetti et al. 2010, 2012). So far, about 200 galaxy-sized strong lensing systems have been discovered (e.g., Bolton et al. 2008). The constraints on the mass fraction of subhaloes in galaxies have been investigated (e.g., Xu et al. 2009). However, the number of strong lensing systems with high quality imaging observations is still limited. Furthermore, strong lensing effects can only probe the very central region of galaxies. Therefore it is not easy to obtain a general understanding about subhaloes from strong lensing effects alone.

Because most of the satellite galaxies are thought to reside in subhaloes, galaxy-galaxy lensing can be an effective way to probe subhaloes statistically. While it was first developed to estimate the dark matter distribution of massive systems, the recent advance of wide and deep surveys,

---

* E-mail:ranl@bao.ac.cn

such as the Sloan Digital Sky Survey (SDSS) [1] and the Canada-France-Hawaii Telescope Legacy Survey (CFHTLS) [2], has allowed applications of galaxy-galaxy lensing analyses to study the mass distributions around lens galaxies of different luminosities, stellar masses, colors, and morphological types (e.g., Brainerd et al. 1996; Hudson et al. 1998; Hoekstra et al. 2003; Hoekstra 2004; McKay et al. 2001; Mandelbaum et al. 2005, 2006, 2008; Sheldon et al. 2009; Johnston et al. 2007). Several studies have investigated the potential of using galaxy-galaxy lensing to probe the masses and density profiles of dark matter subhaloes(e.g., Yang et al. 2006; Li et al. 2009; Pastor Mira et al. 2011). Current observations can only set partial constraints on subhalo properties for individual massive clusters of galaxies (e.g., Limousin et al. 2007; Natarajan et al. 2007, 2009). However, with the next generation of large surveys, such as the Large Synoptic Survey Telescope (LSST) [3], the surface number density of source galaxies that can be used for galaxy-galaxy lensing analyses can reach $n_g \sim 50$ arcmin^{-2}, in comparison with $n_g \sim 1$ arcmin^{-2} for SDSS. This will significantly increase the signal-to-noise of the lensing signal of dark matter subhaloes, thus enabling direct measurements of their masses and density profile.

The goal of this paper is to examine the potential of using galaxy-galaxy lensing to constrain the properties of dark matter subhaloes, such as their mass and density profile. The subhalo properties of satellite galaxies with some fixed property (i.e., stellar mass) are likely to depend on both host halo mass and the location of the satellite galaxy within that host halo. In order to be able to probe these dependencies, we need to distinguish satellite galaxies located in different haloes and at different radii from the centers of their host haloes. One way to do this is to select lens galaxies using a galaxy group catalog (Yang et al. 2006; Johnston et al. 2007; Sheldon et al. 2009; Li et al. 2009). This allows one to select as lenses a subset of satellite galaxies that reside in haloes (groups) of similar mass, and that are at similar (projected) distances from their halo (group) center. In Li et al. (2009), we applied such a method to predict galaxy-galaxy lensing effects for lens galaxies of different luminosities and different morphological types using a group catalog constructed by Yang et al. (2007, hereafter Y07) from the SDSS. The predictions are found to agree well with lensing observations of SDSS from Mandelbaum et al. (2006), demonstrating the validity of the method. In this paper, we use the same methodology to predict the galaxy-galaxy lensing effects for satellite galaxies selected from the SDSS-DR7 group catalog. We investigate the corresponding signal detectability with current and next generation surveys. Employing a Markov Chain Monte Carlo (MCMC) method, we further explore the possibility of constraining both the subhalo and host halo properties in lensing observations at different noise levels expected from different surveys.

This paper is organized as follows. We provide a brief description of the galaxy-galaxy lensing basics in Section 2, and discuss the modeling method in Section 3. In Section 3.1, we introduce the group catalog, SDSSGC, from which lens galaxies are selected. In Sections 3.2 and 3.3, we describe our models for the dark matter distribution around galaxies. In Sections 4 and 5, we show the results and examine the detectability of the predicted lensing signals in SDSS-like and LSST-like surveys. We discuss some systematic bias in our method, and how to correct for it, in Section 6. Section 7 contains a summary.

Throughout the paper, we adopt a ΛCDM cosmology with parameters given by the WMAP-7-year data (Komatsu et al. 2010).

2 GALAXY-GALAXY LENSING

Galaxy-galaxy lensing measures the tangential shear, $\gamma_t(R)$, azimuthally averaged over a thin annulus at the projected radius R around the lens galaxies. In the weak lensing regime, this quantity is related to the excess surface density, $\Delta\Sigma$ (hereafter ESD) through the relation

$$\Delta\Sigma(R) = \gamma_t(R)\Sigma_{\rm crit} = \bar{\Sigma}(< R) - \Sigma(R)\,, \tag{1}$$

where $\bar{\Sigma}(< R)$ is the average surface mass density within R, and $\Sigma(R)$ is the azimuthally averaged surface density at R. It is noted that there is no mass-sheet degeneracy here, and $\Delta\Sigma(R)$ is independent of a uniform background. In the above equation,

$$\Sigma_{\rm crit} = \frac{c^2}{4\pi G}\frac{D_s}{D_l D_{ls}(1+z_l)^2} \tag{2}$$

is the critical surface density in comoving units, with D_s and D_l the angular diameter distances to the lens and to the source, D_{ls} the angular diameter distance between the lens and the source, and z_l the redshift of the lens.

The lensing signal around a galaxy is determined by the projected density profile around it. On average, the surface mass density, $\Sigma(R)$, is related to the line-of-sight projection of the galaxy-matter cross-correlation function, $\xi_{\rm g,m}(r)$. Under the approximation that lenses are at distances much larger than R, we can write

$$\Sigma(R) = \bar{\rho}\int\left[1+\xi_{\rm g,m}(\sqrt{R^2+\chi^2})\right]\,d\chi\,; \tag{3}$$

and

$$\Sigma(< R) = \frac{2}{R^2}\int_0^R \Sigma(u)u du, \tag{4}$$

where $\bar{\rho}$ is the mean density of the universe and χ is the comoving radial distance along the line of sight.

The lensing signal around a satellite galaxy depend sensitively on its location in the host dark matter halo (Yang et al. 2006; Li et al. 2009). The $\Sigma(R)$ around a central galaxy, which mostly resides at the center of the host dark matter halo, is dominated by the density profile of its host halo. On the other hand, the lensing signal of a satellite galaxy, which orbits around in the host halo, consist of two parts. On small scales, the signal is dominated by the subhalo associated with the satellite itself. On larger scales, however, the lensing signal is mainly due to the host halo. We therefore need to model the density profiles of both host haloes and subhaloes.

When calculating the surface mass density around a satellite, we neglect the contributions from other subhaloes. This approximation should not lead to large errors because the fraction of mass contained in subhaloes is only about 10% of the total mass of the host halo (e.g. van den Bosch et al. 2005; Springel et al. 2008; Giocoli et al. 2010). For a single halo, these substructures produce small fluctuations on the host halo profile. However, in galaxy-galaxy lensing analysis, one stacks the lensing signal around many lens galaxies, and the net contribution from subhaloes other than the ones associated with the satellite galaxies themselves is averaged out and included in the host halo profile. In the model calculation, we also neglect the two-halo term, specifically, the contribution to the lensing signal from other haloes in the foreground and background. Our previous studies (Li et al. 2009; Cacciato et al. 2009) calculate this contribution with different methods, and show that the two-halo term is completely negligible on the scales of individual haloes we are concerned with here.

---

[1] http://www.sdss.org
[2] http://www.cfht.hawaii.edu/Science/CFHLS/
[3] http://www.lsst.org/

3 MODELING THE STRUCTURE OF DARK MATTER HALOES

In this paper, we adopt the same methodology as that used in Li et al. (2009) to model the galaxy-galaxy lensing signal around a sample of satellite galaxies. In the following subsections, we describe briefly the galaxy and group catalogs, and our models for the mass distributions around satellite galaxies.

3.1 Galaxy groups

In Li et al. (2009), we used the SDSS DR4 group catalog (Yang et al. 2007). Here we use an updated version of this catalog [4] (hereafter SDSSGC) based on the SDSS DR7 (Abazajian et al. 2009). The group catalog is constructed with the adaptive halo-based group finder developed by Yang et al. (2005, 2007) using galaxies with spectroscopic redshifts in the range of $0.02 \leqslant z \leqslant 0.2$. The redshift completeness is $\mathcal{C} > 0.7$. Three group samples with different sources of galaxy redshifts have been constructed. Our analysis is based on Sample II, which consists of 599301 galaxies with redshift from the SDSS and 3269 galaxies with redshift from other sources. There are in total 472113 groups, including those with only one member galaxy.

A key aspect of this group finder is to estimate the halo mass, M, for each group with a ranking method. In SDSSGC, two estimators for halo mass are provided. One is based on the characteristic luminosity of a group, defined to be the total luminosity of all member galaxies with $M_r - 5\log h < 19.5$. The other is based on the characteristic stellar mass, $M_{\rm stellar}$, defined to be the total stellar mass of members galaxies with $M_r - 5\log h < 19.5$. The stellar mass of an individual galaxy is calculated from its luminosity and colors using the fitting formula given by Bell et al. (2003). Y07 showed that the characteristic stellar mass is a better indicator of the halo mass, and thus we adopt this mass estimator throughout the paper.

The basic assumption of the ranking method to assign a halo mass to a group is that there is a one-to-one relation between $M_{\rm stellar}$ and the halo mass. Once a theoretical dark matter halo mass function is adopted, one can establish a relation between halo mass, M, and $M_{\rm stellar}$ so that the number of haloes with masses above M is equal to the number of groups with characteristic stellar mass above $M_{\rm stellar}$. A group with a given $M_{\rm stellar}$ is then assigned the corresponding halo mass M. Clearly, this one-to-one mapping requires the group sample to be complete. Therefore, we only use complete samples of groups in the SDSSGC in our ranking. The masses of other groups are estimated using linear interpolation based on the $M_{\rm stellar}$ -M relation obtained from the complete sample. We refer readers to Yang et al. (2007, 2008) for details about the group catalog construction and the halo mass assignment. According to Y07, the uncertainty in the mass assignment is about 0.2-0.3 dex for groups considered in this paper. This uncertainty will not change our results significantly because the considered lensing signals are the average signals over a statistical sample of galaxies. We have tested the effect by performing calculations with group mass to which an artificial 0.3 dex log-normal error is added. This uncertainty brings negligible change in our results. Note that the halo mass assigned to a group in the SDSSGC is M_{200}, which is the mass enclosed in the radius, r_{200}, defined such that $M_{200} = 4\pi r_{200}^3(200\bar{\rho})/3$. For consistency, we convert M_{200} to our definition of halo mass (see Eq. [7] below) using the conversion method described in the appendix of Hu & Kravtsov (2003).

3.2 Host halo density profile

We assume that the host dark matter halo of each group is centered on the most massive group member, to which we refer as the central galaxy. The dark matter host haloes are assumed to follow the NFW (Navarro et al. 1997) profile,

$$\rho_{\rm dm}(x) = \begin{cases} \frac{\delta_0 \rho_{\rm crit}}{x(1+x)^2} & \text{if } x \leqslant c \\ 0 & \text{else} \end{cases} ,$$

where $x \equiv r/r_s$, with r_s being the characteristic scale of the halo and related to the halo virial radius $r_{\rm vir}$ through the concentration parameter $c = r_{\rm vir}/r_s$, and $\rho_{\rm crit}$ is the critical density of the universe. The characteristic over-density δ_0 is related to the average over-density of a virialized halo, $\Delta_{\rm vir}$, by

$$\delta_0 = \frac{\Delta_{\rm vir}}{3} \frac{c^3}{\ln(1+c) - c/(1+c)} . \tag{5}$$

For the ΛCDM model considered here, we adopt the parametric form of $\Delta_{\rm vir}$ given by Bryan & Norman (1998) based on the spherical collapse model,

$$\Delta_{\rm vir} = 18\pi^2 + 82[\Omega(z) - 1] - 39[\Omega(z) - 1]^2 , \tag{6}$$

where $\Omega(z)$ is the cosmological density parameter at redshift z. The viral mass of a halo can then be written as:

$$M = \frac{4\pi}{3} r_{\rm vir}^3 \Delta_{\rm vir} \rho_{\rm crit} . \tag{7}$$

It is seen that given the mass of a halo, its density profile depends only on the concentration parameter c. Numerical simulations show that at a given redshift, c decreases gradually with halo mass (e.g., Bullock et al. 2001; Eke et al.

---

[4] http://gax.shao.ac.cn/data/Group.html

2001). However the exact mass dependence of the concentration parameter has not yet been well constrained by observations. Various fitting formulae have been proposed on the bases of numerical simulations (e.g., Bullock et al. 2001; Zhao et al. 2003; Dolag et al. 2004; Macciò et al. 2007; Zhao et al. 2009). Since the difference between these different fitting functions does not affect our results qualitatively, we adopt the fitting formula of Bullock et al. (2001),

$$c = \frac{c_*}{1+z}\left(\frac{M}{10^{14}\mathrm{h}^{-1}\mathrm{M}_\odot}\right)^{-0.13}, \qquad (8)$$

where $c_* \approx 8$ for the ΛCDM cosmology considered here. Although simulations indicate a scatter of ~ 0.1dex in this concentration mass relation (e.g. Jing 2000; Bullock et al. 2001; Wechsler et al. 2002; Macciò et al. 2007), we ignore this scatter in our analysis. We have verified that adding scatter has no significant impact on any of our results.

To obtain galaxy-galaxy lensing signals around a halo center, we need to project the 3-D mass distribution. According to Hamana et al. (2004), the ESD can be written as

$$\Delta\Sigma(y) = 2\Delta\Sigma_s f(y)\,, y = \frac{R}{r_s}\,, \qquad (9)$$

where $\Delta\Sigma_s = \rho_s r_s$. For the NFW profile, the dimensionless function $f(y)$ can be written as (Wright & Brainerd 2000; Bartelmann 1996)

$$f(y) = \begin{cases} \frac{1}{(y^2-1)}\left(1 - \frac{\ln\left(\frac{1+\sqrt{1-y^2}}{y}\right)}{\sqrt{1-y^2}}\right) & \text{if } y<1\,, \\ \frac{1}{3} & \text{if } y=1, \\ \frac{1}{(y^2-1)}\left(1 - \frac{\mathrm{atan}\sqrt{y^2-1}}{\sqrt{y^2-1}}\right) & \text{if } y>1\,. \end{cases} \qquad (10)$$

Note that the above equation assumes that the NFW profile extends infinitely without a truncation at the virial radius. We have tested that the difference between truncated and non-truncated profiles has negligible impact on our results.

3.3 Subhalo density profile and mass distribution

In order to assign a subhalo mass to a satellite galaxy we use the evolved subhalo mass function of van den Bosch et al. (2005), which describes the abundance of subhaloes as function of their evolved, present-day mass. Specifically, for each satellite galaxy, we assume that the mass of its subhalo at accretion (i.e., its un-evolved mass) is related monotonically to its stellar mass. The retained mass fraction of the subhalo after evolution in the host halo can be described by a parameter f_m. Gao et al. (2004) analyzed the radial dependence of f_m from a large sample of subhaloes in cosmological simulations, and showed that

$$f_m = 0.65(r_{\rm dis}/r_{\rm vir})^{2/3}\,, \qquad (11)$$

where $r_{\rm dis}$ is the distance of the subhalo from the center of the host halo, and $r_{\rm vir}$ is the virial radius of the host halo. Observationally, the line-of-sight distance cannot be estimated accurately, and only the projected halo-centric distance, $r_{\rm p}$, can be used. We then adopt the following approach to estimate the three-dimensional distance of the satellite. For a satellite with a given $r_{\rm p}$, we randomly sample a 3-D halo-centric distance assuming that the spatial distribution of the satellites follows the NFW profile, and use this distance in equation (11) to estimate f_m. With f_m, we can define a ranking parameter $\mathcal{Q}$ for every member satellites in a group with host halo mass M as

$$\mathcal{Q} = f_m M_*\,, \qquad (12)$$

where M_* is the stellar mass of the satellite galaxy. We then generate a set of subhalo masses for a given host halo mass M using the fitting formula for the evolved subhalo mass function of van den Bosch et al. (2005). Finally, by ranked mapping, a subhalo mass is assigned to a satellite according to its ranking parameter $\mathcal{Q}$.

Fig.1 shows the results of our subhalo mass assignment. The upper panels are the stellar mass distributions for the satellites with their host halo mass in the range indicated in the plots. We split satellites into sub-samples according to their projected halo-centric distance r_p shown by different lines. One can find that the peak of the stellar mass distribution does not depend strongly on their projected distance. The mass distributions of the correspondng subhaloes are shown in the lower panels. The average mass to light ratio is about 10.

We model the density profile of subhaloes with a truncated NFW profile

$$\rho_{sub}(r) = \begin{cases} f_t\rho_{i,sub}(r) & \text{if } r \leqslant r_t, \\ 0 & \text{if } r > r_t \end{cases} \qquad (13)$$

where $\rho_{i,sub}(r)$ is the NFW profile corresponding to the mass of the subhalo at the time of its accretion into its host. The parameter f_t is a dimensionless factor describing the reduction in the central density, and r_t is a cut-off radius imposed by the tidal force of the host halo. In $\rho_{i,sub}(r)$, the characteristic scale and density are denoted by $r_{\rm s,sub}$ and $\delta_{0,sub}$, respectively. Note that the parameters of f_t and $\delta_{0,sub}$ can be combined to a single parameter denoted by $\rho_{0,\rm sub}$. For $f_t = 1$ and $r_t \gg r_{\rm s,sub}$, $\rho_{sub}(r)$ approaches to the standard NFW profile $\rho_{i,sub}(r)$. For the cut-off radius r_t, we use the analytical tidal radius formula (Binney & Tremaine 1987; Tormen et al. 1998),

$$r_t = \left(\frac{M_{\rm sub}}{(2 - d\ln M/d\ln r)M(<r_{\rm dis})}\right)^{1/3} r_{\rm dis}\,, \qquad (14)$$

where $M(<r_{\rm dis})$ is the host halo mass within a sphere of radius $r_{\rm dis}$. As shown by Springel et al. (2008), this analytical prediction agrees well with the trunctation radii of dark matter subhaloes N-body simulations. The density profile is normalized to the mass assigned to the subhalo by choosing a proper f_t (or equivalently $\rho_{0,\rm sub}$) . Therefore in our model the mass profile assigned to a subhalo is specified by three quantities: (i) the stellar mass of the satellite galaxy; (ii) the host halo mass; and (iii) the distance between the satellite and the center of the host halo.

It should be pointed out that there are still substantial uncertainties in modeling the mass distribution around individual satellite galaxies. In particular, many of the results about subhaloes are obtained from pure N-body simulations. It is unclear how significant the effect of including baryonic matter is. However, the aim of this work is to investigate to what extent current and future lensing data can constrain the density distribution of dark matter subhaloes. Our relatively simple model for the density distribution of subhaloes should be sufficient for this purpose.

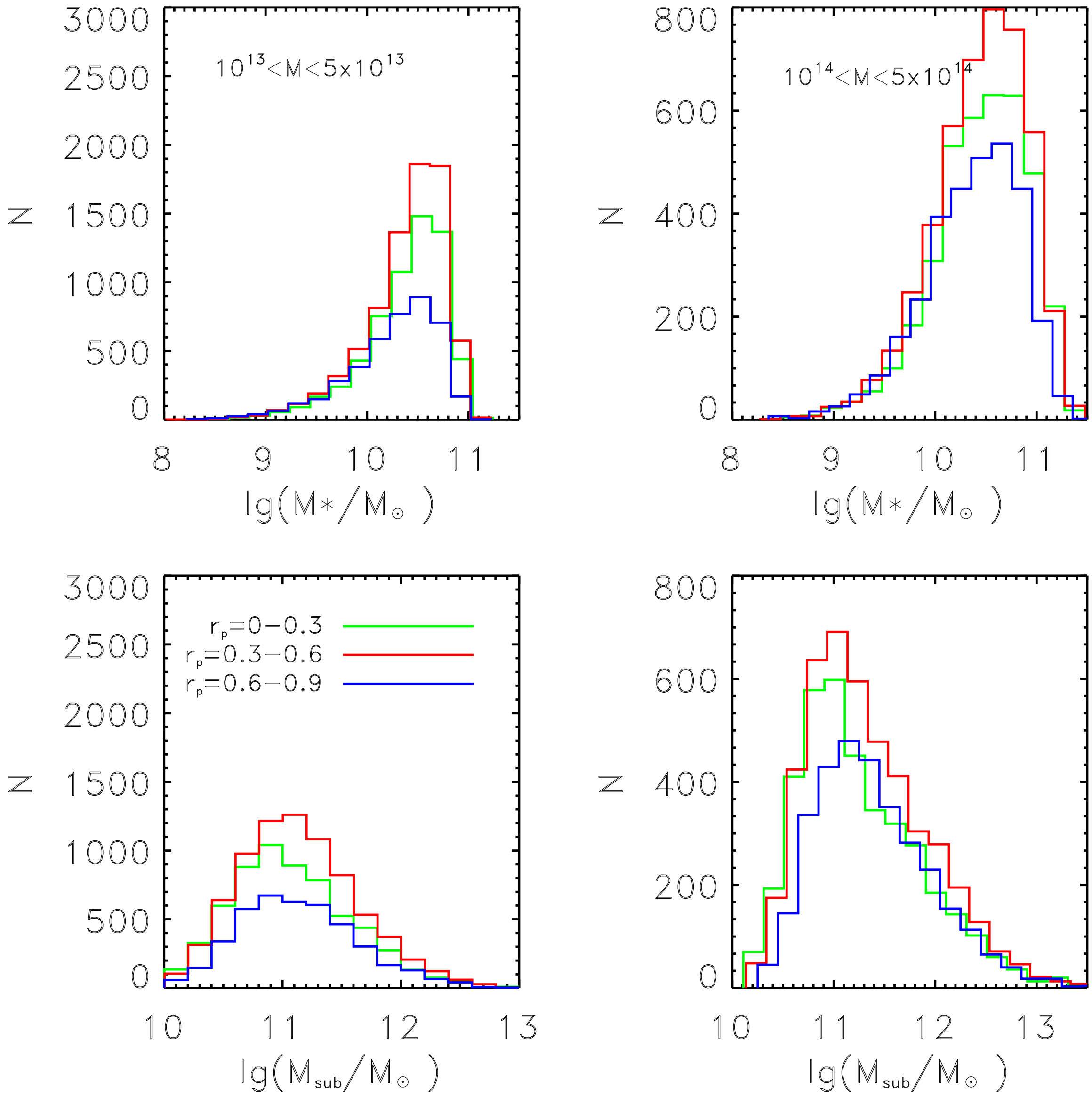

Figure 1. The figure shows the stellar mass and subhalo mass distribution of satellite galaxies with host halo mass in certain ranges. The host haloes mass range are $[10^{13}, 5 \times 10^{13}]\mathrm{h}^{-1}\mathrm{M}_\odot$ for left panels and $[10^{14}, 5 \times 10^{14}]\mathrm{h}^{-1}\mathrm{M}_\odot$ for right panels. In the upper panels of the figure, we plot the stellar mass distribution for the satellites. We split the satellites into sub-samples according to their projected halo-centric distance r_p and plot the stellar mass distribution of these sub-sample with different color. The respective r_p range for each color of the line is marked in bottom left panel in unit of r_vir. In the lower panels, we plot the mass distribution for the subhaloes for corresponding satellites sample.

4 MODELLED LENSING SIGNAL

4.1 Lensing signal of individual satellite

We first calculate the behavior of galaxy-galaxy lensing signal as a function of the projected radius around a single satellite. Similar results can be found in, e.g. Yang et al. (2006) and Li et al. (2009). In Fig.2, we plot $\Delta\Sigma(R)$ for satellites of different mass and at different position in a host halo with mass of $M = 10^{14}\mathrm{h}^{-1}\mathrm{M}_\odot$. In the left panel, the subhalo mass is set to be zero to show the lensing signal contributed by the host halo alone. Different lines show the predictions for satellites located at different projected halo-centric distances, r_p. It is clear that the contribution from the host halo depends strongly on the position of the satellite. For $r_p = 0$, i.e., the central galaxy, $\Sigma(R)$ is just the projection of NFW density profile, and $\Delta\Sigma(R)$ decreases monotonously. For a satellite galaxy with $r_p \neq 0$, however, $\Delta\Sigma(R)$ from the host halo is nearly 0 on small scales around the satellite. This is because the host halo density varies smoothly on small scale around the satellite. As R grows, $\Delta\Sigma(R)$ decreases to negative values, reaching a minimum at $R = r_p$ where the outer annulus in Eq.(1) reaches the centre of the host halo. It then goes up rapidly, eventually approaching the $\Delta\Sigma(R)$ profile for the central galaxy. In the right panel, we show $\Delta\Sigma(R)$ for satellites at $r_p = 0.5\mathrm{h}^{-1}\mathrm{Mpc}$ with different subhalo mass. Clearly subhalo dominates the inner part of the ESD profile. The value of $\Delta\Sigma(R = 0.01\mathrm{h}^{-1}\mathrm{Mpc})$ increases by a factor of 2.5 when the subhalo mass increases from $10^{11}\mathrm{h}^{-1}\mathrm{M}_\odot$ to $10^{12}\mathrm{h}^{-1}\mathrm{M}_\odot$.

4.2 Stacking

Observationally, weak lensing signals are derived by accurately measuring the shape of the light distribution of source galaxies. The intrinsic shape of source galaxies then contributes significant noise to the lensing signal. Specifically, the measured tangential ellipticity e_+ of a source galaxy is related to the lensing tangential shear γ_t acting upon it by

$$e_+ = 2\gamma_t\mathcal{R} + e_+^{int}\,, \tag{15}$$

where e_+^{int} is the intrinsic tangential ellipticity of the source galaxy and $\mathcal{R}$ is the "responsivity", reflecting how the shape of a galaxy responds to the shear applied to it (Bernstein & Jarvis 2002). This quantity can be determined from observational data, and we set $\mathcal{R} = 0.87$ following Mandelbaum et al. (2006). In galaxy-galaxy lensing, one suppresses the noise arising from the intrinsic shape of source galaxies by combining shape information from as many source images as possible. Unless the density of background source is extremely high, this typically requires also stacking the signal from many lens galaxies. Assuming no intrinsic alignment for source galaxies, the averaged intrinsic ellipticity over many galaxies is expected to approach zero. Thus the average of e_+ gives rise to an unbiased estimate of $2\gamma_t\mathcal{R}$. The corresponding uncertainty of the tangential shear measurement can be written as

$$2\mathcal{R}\sigma_\gamma = \sqrt{\sigma_{SN}^2 + \sigma_e^2}/\sqrt{N_{pair}}\,, \tag{16}$$

where N_{pair} is the number of lens-source pairs, $\sigma_{SN} \approx 0.3$ is the source galaxy intrinsic shape dispersion for one component of the ellipticity, and σ_e is the measurement noise for one component of the ellipticity. The measurement noise can originate from photon noise and inaccurate PSF corrections. For the SDSS, σ_e falls in the range from 0.05 to 0.4, depending on the luminosity of the source galaxies (Mandelbaum et al. 2005). Throughout this paper, we adopt $\sigma_e = 0.2$. It should be pointed out that the LSST will improve significantly in survey depth and angular resolution compared to SDSS, and thus σ_e is expected to be much smaller. The measurement noise adopted here is therefore a very conservative estimate for future surveys. We fix the lens redshift to be $z_l = 0.15$, which is the mean redshift of galaxies in the SDSSGC. For source galaxies, we consider two models. The first model (hereafter LEV1) is for SDSS-like surveys, which, to a certain extent, represents the current state-of-the-art for large surveys. The second model (hereafter LEV2) is for future LSST-like surveys. For LEV1 and LEV2 the source galaxy redshift is taken to be $z_s = 0.3$ and $z_s = 1$, respectively. For simplicity, we do not consider detailed redshift distributions for source and lens galaxies. This may lead to inaccurate predictions for lensing signals, especially for LEV1 with relatively low z_s. However, for the purpose of comparing the detectibillity of LEV1 and LEV2 surveys, our simplification should be adequate. On the other hand, for future studies requiring high precision, the redshift distributions of source and lens galaxies has to be properly accounted for.

With fixed z_l and z_s, we have

$$\sigma_{\Delta\Sigma}(R) = \sigma_\gamma(R) \times \Sigma_{crit}(z_l, z_s)\,. \tag{17}$$

Thus the lensing measurement noise only depends on N_{pair}, which in turn is determined by the number of lens galaxies and the number density of source galaxies. We use the SDSSGC to estimate the number of lens galaxies. Fig.3 shows the number of lens galaxies in SDSSGC as a function of the projected group-centric radius for different halo mass range. Typically the SDSSGC provides between 2000 and 6000 satellite galaxies (= lenses) per bin in host halo mass and group-centric radius, for the binning adopted here. When halo mass decreases, the number of groups keeps increasing, but the number of satellites per host goes down. At halo mass range of $10^{13} - 10^{14}\mathrm{h}^{-1}\mathrm{M}_\odot$, one obtains largest number of lens galaxies.

Future surveys such as LSST will include spectroscopic data, making it difficult to construct a reliable group catalog from the survey data itself. This will have to await future deep and wide spectroscopic surveys which will allow the construction of very large group catalogs, out to high redshifts. This would allow the galaxy-galaxy lensing based subhalo studies proposed here to be extended to higher redshifts, using tomography. An alternative is to consider using photometric redshifts for the construction of group catalogs. We leave these avenues for future investigation. In what follows we simply adopt the lens statistics from the SDSSGC for both LEV1 and LEV2; i.e., even for LEV2, we still only consider groups constructed from relatively shallow SDSS-like spectroscopic surveys. Finally, for the number density of source galaxies we adopt 1.6 arcmin^{-2} for LEV1 (as appropriate for SDSS, see Mandelbaum et al. 2005) and 60 arcmin^{-2} for LEV2.

In Fig.4, we compare the lensing measurement noise for LEV1 and LEV2, respectively. We calculate average lensing signals around satellite galaxies with host halo mass in the range of $[10^{14}, 5\times10^{14}]\mathrm{h}^{-1}\mathrm{M}_\odot$ and $[10^{13}, 5\times10^{13}]\mathrm{h}^{-1}\mathrm{M}_\odot$ and with halo-centric distance in the range of $[0.1, 0.2]$ and $[0.5, 0.6]$ $\mathrm{h}^{-1}\mathrm{Mpc}$. We plot the expected noise from our two noise models, LEV1 and LEV2, with red and blue error bars, respectively. It is seen that both the SDSS-like survey and the LSST-like survey can detect the lensing signal from the host halo well. For the inner parts where the subhaloes dominate, the observational noise from SDSS-like survey is much larger than the signal. On the other hand, a LSST-like survey can detect the signal with high S/N. The S/N does not drop for smaller groups, because the number of smaller groups is much larger than that of massive ones and the mean subhalo mass does not drop significantly in smaller groups (see Fig.1).

5 MODEL INFERENCE WITH THE MARKOV CHAIN MONTE CARLO METHOD

5.1 Markov Chain Monte Carlo fitting

For a given set of observational data θ, the posterior probability of the model parameters π can be derived from the likelihood function, $\mathcal{L}(\theta|\pi)$, and the prior probability, $P(\pi)$,

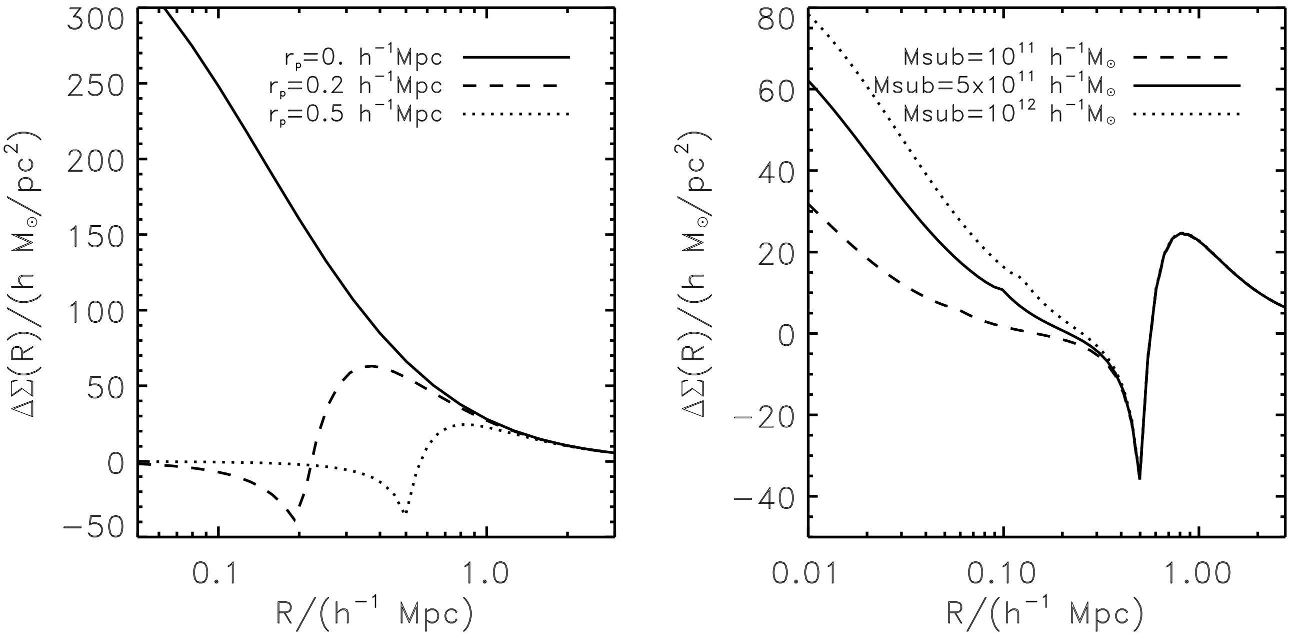

Figure 2. In left panel, we plot the lensing signal around satellites at different positions in the halo of $10^{14}h^{-1}M_\odot$. The satellite mass is set to zero. Different lines represent different projected halo-centric distance. In the right panel, different lines represent lensing signal around satellites of different mass within a host halo of $10^{14}h^{-1}M_\odot$.

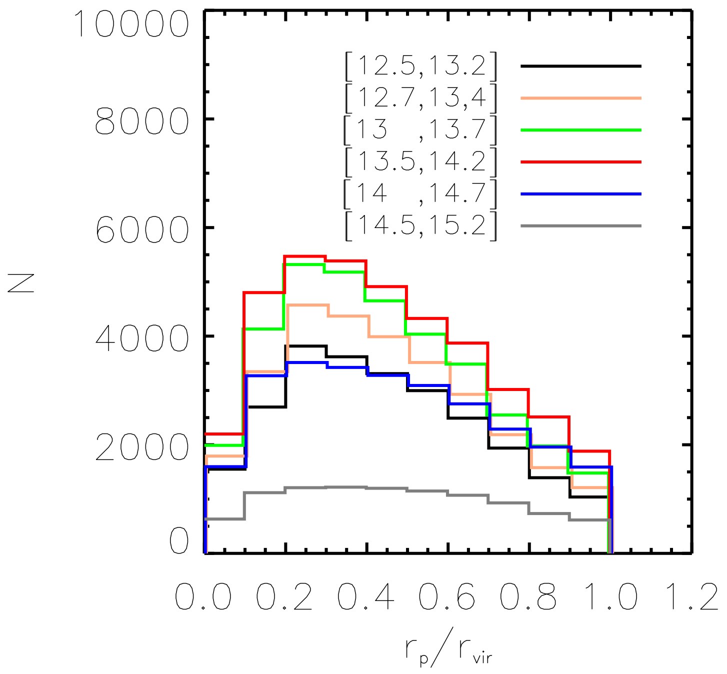

Figure 3. The figure shows the number of galaxies in SDSSGC as function of projected group-centric radius. Different line styles represent different host halo mass. The respective ranges of $\log(M/h^{-1}M_\odot)$ are marked in the figure.

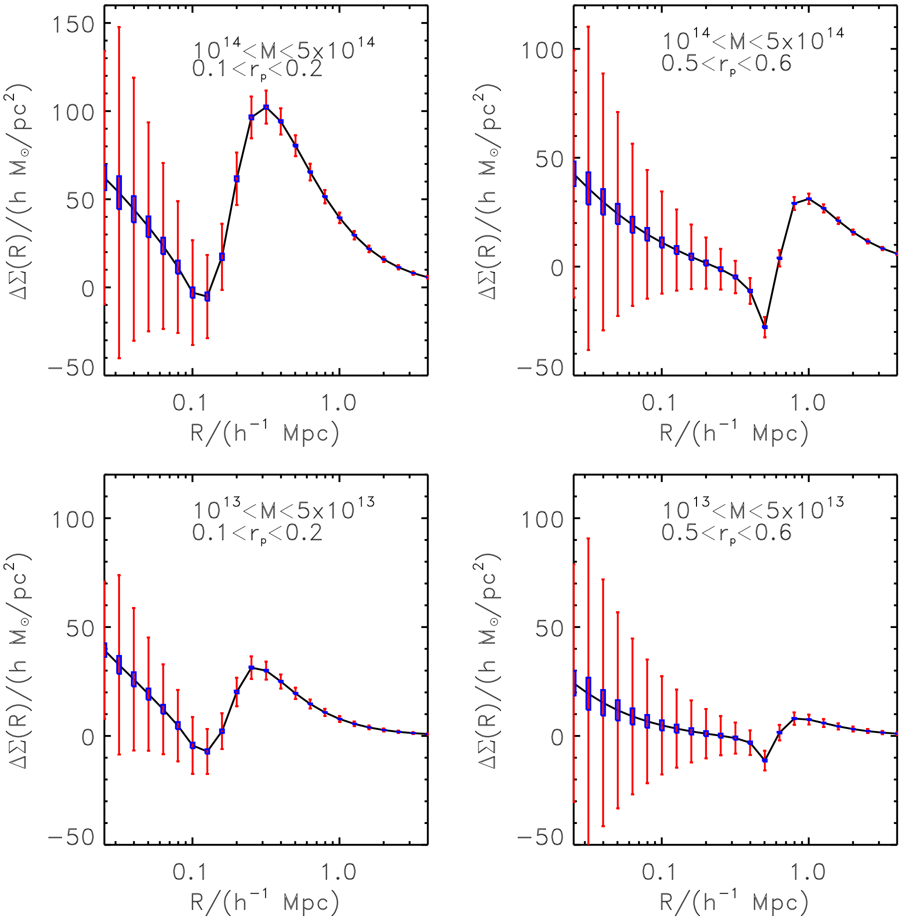

Figure 4. In this figure, we plot the galaxy-galaxy lensing signal around satellites in certain host halo mass bins and projected distance bins and compare it with the noise estimation. The red errorbars show the noise estimation of LEV1(SDSS like survey), while the blue rectangles show the LEV2 noise(LSST like survey).

of these parameters. According to Bayes' rule, we can write

$$P(\pi|\theta) = \frac{\mathcal{L}(\theta|\pi)P(\pi)}{P(\theta)}, \tag{18}$$

where the normalization, $P(\theta)$, is called the evidence. The prior probability $P(\pi)$ describes our known knowledge about the model parameters. In our fiducial computation, we simply adopt a flat prior over a range in the parameter space. As a test of the robustness of our inferences, we also use another set of priors. We write the likelihood function $\mathcal{L}$ as

$$\ln\mathcal{L} = \sum_i \left(\frac{\Delta\Sigma(R_i|\pi) - \Delta\hat{\Sigma}(R_i)}{\sigma_{\Delta\Sigma}}\right)^2, \tag{19}$$

where $\Delta\hat{\Sigma}(R_i)$ is the observed excess surface density at radius bin R_i and $\Delta\Sigma(R_i|\pi)$ the theoretical prediction with model parameters π. In this paper, we use MCMC to explore the posterior distribution $P(\pi|\theta)$. The key component of the MCMC method is a guided random walk in the parameter space. The likelihood function at a certain volume of the parameter space is then proportional to the number density of points in that volume. The MCMC sampler used here is that provided in the CosmoMC package (Lewis & Bridle 2002), which adopts the Metropolis-Hastings algorithm (Metropolis & Ulam 1949; Metropolis et al. 1953; Hastings 1970) by default. A detailed review of this method can be found in Chib & Greenberg (1995). For each fitting process, we generate three MCMC chains starting from different positions in the parameter space. We use the runtime convergence criteria in CosmoMC, which computes the standard Gelman and Rubin R-statistic diagnostics to monitor the convergence. We declare convergence when $R < 1.1$. Only the second half of the chain values are used to sample the posterior probability.

5.2 Model inference

Here we investigate to what extent the observations of satellite galaxy-galaxy lensing from LEV1 and LEV2 surveys can constrain the satellite and host halo properties described by a set of parameters, including (M, c, r_p) for the host halo and $(M_{\rm sub}, \rho_{0,\rm sub}, r_{\rm s,sub})$ for the subhalo. We construct the 'observed' galaxy-galaxy lensing signals for satellites selected from SDSSGC following the descriptions in §4. We consider separately two subsamples of satellites according to their host halo mass, one in the range of $[10^{14}, 5\times10^{14}]\rm h^{-1}M_\odot$ (SAMPLE1), and the other for $[10^{13}, 5\times10^{13}]\rm h^{-1}M_\odot$ (SAM-

Table 1. The mean values of parameters for the input galaxies, and the boundary of the parameter space adopted in the MCMC. M and $M_{\rm sub}$ are in units of $\rm h^{-1}M_\odot$; $r_{\rm p}$ and $r_{\rm s,sub}$ are in units of $\rm h^{-1}Mpc$; $\rho_{\rm 0,sub}$ is in units of $10^{16}h^2M_\odot{\rm Mpc}^{-3}$.

	$\log M$	c	$r_{\rm p}$	$\log M_{\rm sub}$	$\rho_{\rm 0,sub}$	$r_{\rm s,sub}$
mean input	14.247	6.89	0.55	11.67	0.99	0.0155
high bound	14.5	10	0.6	12	10	0.2
low bound	13.5	3	0.5	9	0.1	0.001

PLE2). The projected halo-centric distances of satellites are chosen to be in the range of $[0.5, 0.6]\rm h^{-1}Mpc$ for both subsamples. We stack the galaxy-galaxy lensing signals for the satellite galaxies in each subsample thus constructing a set of 'observed' signals. We then employ MCMC fitting to these mock data in order to derive constraints on the mean values for the six parameters, three for host haloes (M, c, r_p) and three for subhaloes $(M_{\rm sub}, \rho_{\rm 0,sub}, r_{\rm s,sub})$. The selection of the bin size in the projected halo-centric distance of satellites is a compromise between statistical errors and systematic bias. If we used the bin size of $0.2\rm h^{-1}Mpc$ instead of $0.1\rm h^{-1}Mpc$, for example, the source galaxy number would increase by about a factor of two and thus the statistical errors are decreased. However, that stacking satellites over a larger range in $r_{\rm p}$ leads to larger biases in the derived mean host halo mass M and concentration parameter c from MCMC fitting to the stacked satellite galaxy-galaxy lensing signals.

To derive the parameters we are interested in, we fit the mock lensing data with the model,

$$\Sigma(R) = \Sigma_{\rm host}(R|M, c, r_p) + \Sigma_{\rm sub}(R|M_{\rm sub}, \rho_{\rm 0,sub}, r_{\rm s,sub})\,, \tag{20}$$

where

$$\Sigma_{\rm host}(R|M, c, r_p) = \frac{1}{2\pi}\int_0^{2\pi}\Sigma(\sqrt{r_p^2+R^2+2r_pR\cos\theta})d\theta, \tag{21}$$

where $\Sigma(R)$ is the projected density profile of the NFW host halo with mass M and concentration parameter c. Note that R is the distance to the satellite galaxies around which we detect galaxy-galaxy lensing signals. The second term $\Sigma_{\rm sub}(R)$ is the projected density of the subhalo with profile:

$$\rho_{\rm sub} = \begin{cases} \frac{\rho_{\rm 0,sub}}{(1+r/r_{\rm s,sub})^2(r/r_{\rm s,sub})} & \text{if } r < r_t \\ 0 & \text{if } r > r_t \end{cases}\,. \tag{22}$$

where the truncation radius, r_t, is computed using Eq. (14).

We first analyse SAMPLE1 with relatively massive host haloes. Table 1 shows the mean values of the six parameters of the input sample, and the boundary of the flat priors we adopt in our MCMC fitting.

We separately analyse the constraints expected from LEV1 surveys and LEV2 surveys. Fig.5 shows the marginalized posterior probability distribution for the model parameters for LEV1. The contours indicate the 68% and 95% confidence levels. The last panel in each row shows the marginalized probability distribution for the corresponding parameter, in which the probability distribution (blue histogram) and the average value (vertical line) from the input sample are also shown for comparison. As is evident, even for LEV1 the host halo mass M and concentration parameter c can already be constrained reasonably well. However, the constraints on the subhalo mass are extremely weak, with the 68% confidence range covering two orders of magnitude. For the subhalo density profile, no meaningful constraints can be obtained from LEV1-type surveys.

The results obtained using the LEV2 noise model are shown in Fig.6. Clearly, the factor 50 increase in the number density of source images causes a dramatic improvement in the constraints on the model parameters compared to those in Fig.5. The host halo mass and the concentration parameter can be constrained with high precision. The subhalo mass can also be tightly constrained with a 1σ confidence range of about 0.2 dex. For the amplitude and scale radius of the subhalo density profile, reasonable constraints can be achieved. Note, though, that there is a strong degeneracy between $\rho_{\rm 0,sub}$ and $r_{\rm s,sub}$, as seen from their joint constraints in the fifth panel of the bottom row.

To see more clearly the improvements from LEV1 to LEV2, in Fig.7 we directly compare the marginalized probability distributions for M, c, $M_{\rm sub}$ and $r_{\rm s,sub}$ obtained using the LEV2 (solid) and LEV1 (dashed) noise models. This demonstrates the remarkable potential of the next generation of LSST-like surveys for subhalo studies using satellite galaxy-galaxy lensing.

We also perform the MCMC fitting for SAMPLE2 with group sized host haloes with mass in the range of $[10^{13}, 5\times10^{13}]\ \rm h^{-1}M_\odot$. The results are shown in Fig.8. It is seen that for group sized host haloes and the satellites therein, we can still get good constraints with LEV2 surveys.

5.3 The impact of prior choice

The results above are obtained with flat priors for all parameters. Here we test the impact of prior choice on our inferences of model parameters. Since the groups used here are selected from SDSSGC group catalog, each group has already been assigned an estimated mass. Thus we do have some idea about the mass distribution of the selected groups that may be used as priors in the MCMC fitting. As an approximation, we model the mass distribution with a lognormal function,

$$P(\log M) = \frac{1}{\sqrt{2\pi}\sigma}\exp\left(-\frac{(\log M - \log\bar{M})^2}{2\sigma^2}\right)\,, \tag{23}$$

where $\bar{M}$ is the mean mass of the selected groups, and $\sigma = (\sigma_0+\sigma_1)/\sqrt{N}$, with $\sigma_0 = 0.3$ the mass assignment uncertainty in the SDSSGC, σ_1 the standard deviation of the group mass in logarithmic space, and N the number of selected groups. In Fig.9, we show the constraints using this distribution as the prior for the host halo mass. The left panels show the marginalized posterior distribution of M, and the right panels are for the subhalo mass $M_{\rm sub}$. The upper and lower panels are for LEV2 and LEV1, respectively. The black and blue histograms are the results with flat priors for all the parameters, and the lognormal prior for M and flat priors for the other parameters, respectively. The red lines in the left panels illustrate the lognormal prior distribution for M. For LEV2, because the constraints are already tight, adding the lognormal prior on M does not change the constraints significantly, although it does decrease the bias in M by a small (barely significant) amount. In the case of the LEV1 noise model, the posterior distribution for M is

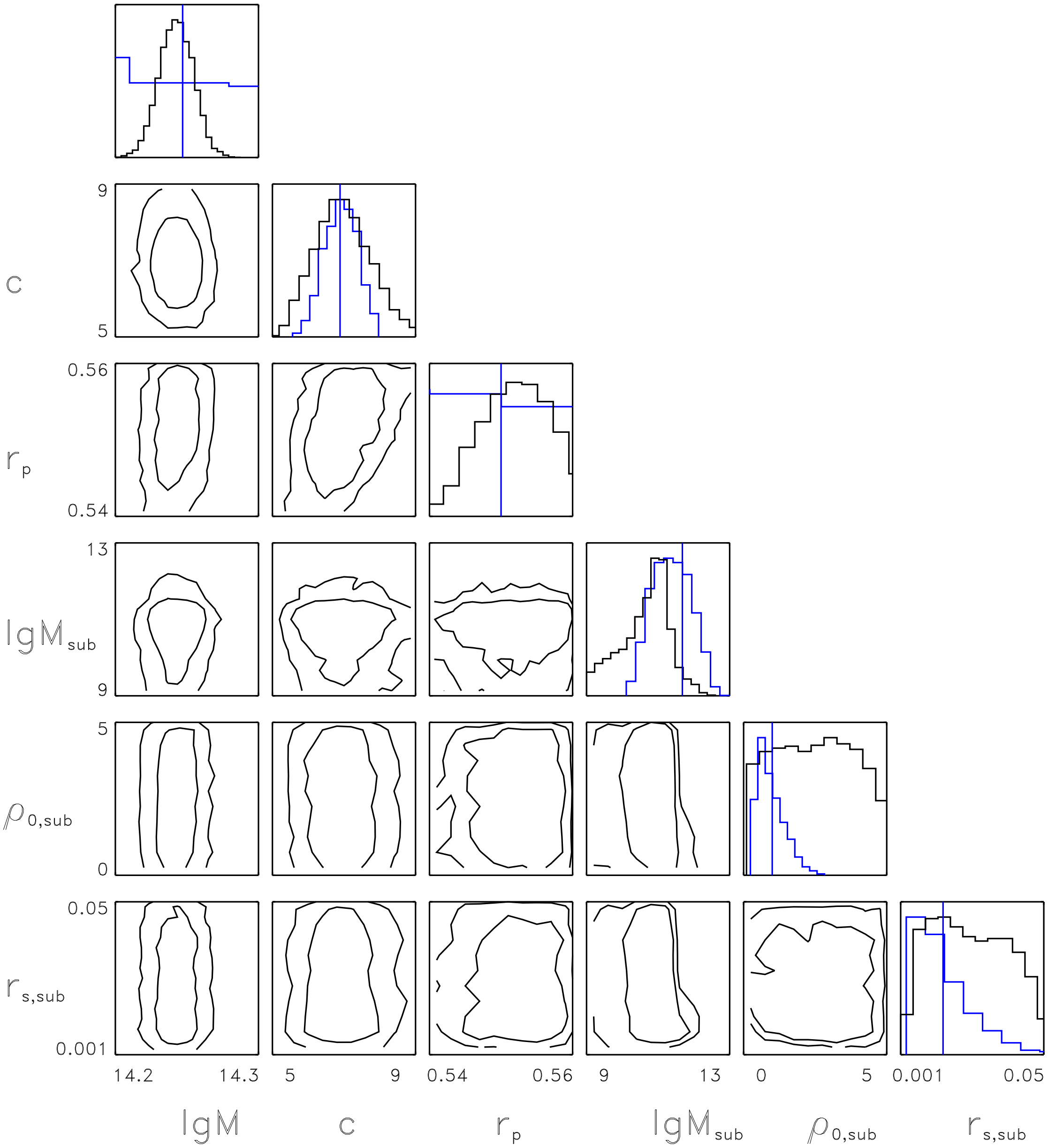

Figure 5. The marginalized posterior probability distribution for the model parameters in LEV1 case. The contours show 68% and 95% confidence levels. The last panel of each row shows the 1-d marginalized probability distribution, together with the average value of the input satellites (vertical solid lines). The blue histograms show the corresponding distributions from the input SAMPLE1.

essentially identical to its prior distribution, indicating that the LEV1 lensing data does not improve the constraints on host halo mass beyond our prior knowledge. For the subhalo mass, the posteriors based on both LEV1 and LEV2 are not affected by the prior on M. This is expected from Figs.5 and 6, which show that the degeneracies between host halo mass and subhalo parameters are very weak.

6 BIAS AND CONTAMINATIONS

6.1 Stacking bias

From Figs.5 and 6, it can be seen that the peak of the posterior distribution for some parameters deviates from the input mean value. These biases are from fitting the model to galaxy-galaxy lensing data obtained by stacking a large sample of satellite galaxies.. The properties of the satellite galaxies and their host haloes in the sample are not identical but spread over certain ranges. The parameters obtained

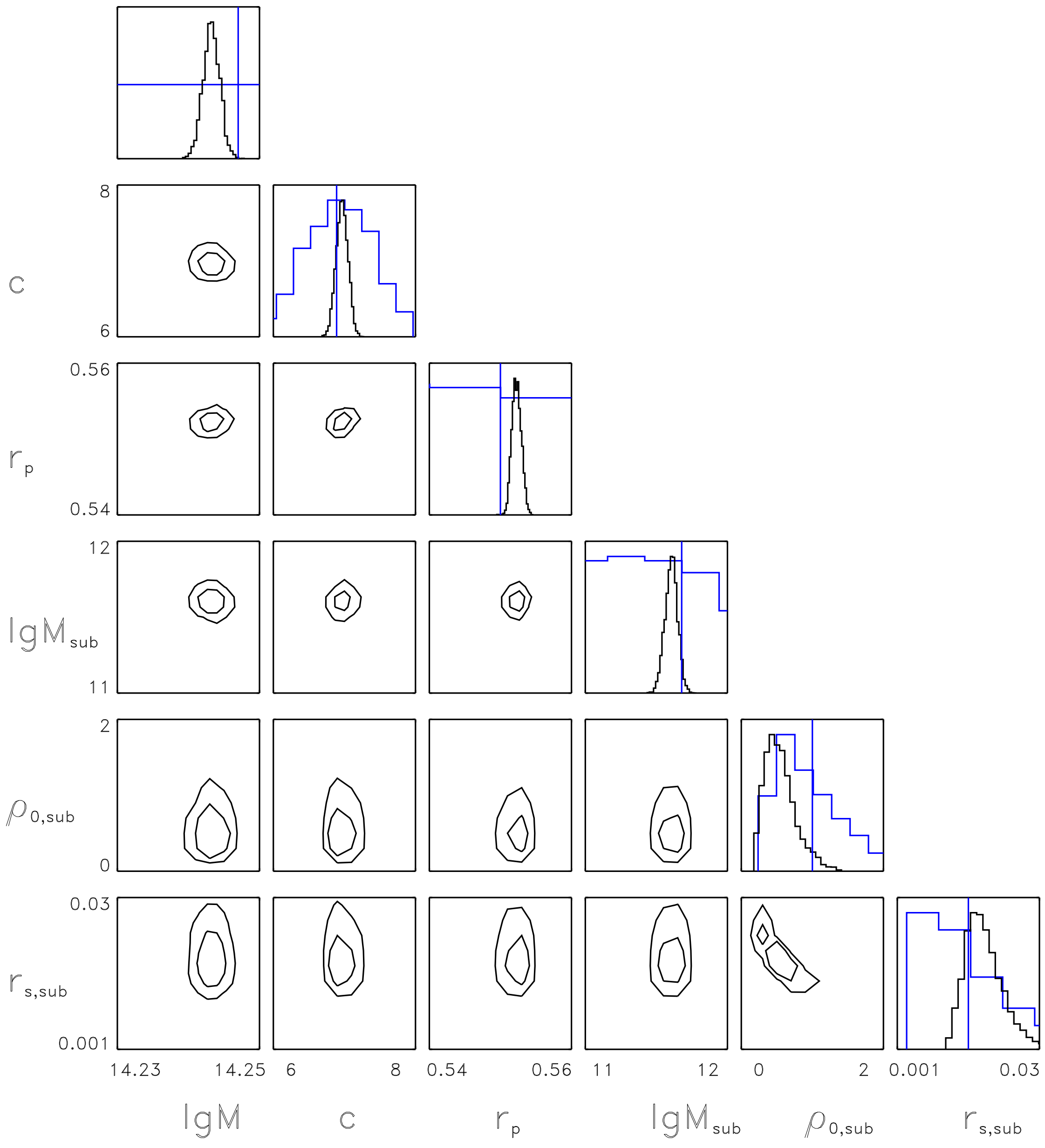

Figure 6. The same as Fig.5 but for results using LEV2 noise model.

from the fitting to the stacked signals then correspond to the results of certain averages over such a sample. Depending on the quantities, the averages obtained may be biased relative to the means of the input values. In our analyses, although the properties of lens galaxies, such as their host halo mass and the halo-centric locations, are selected to be similar, they still cover finite ranges with some distributions. In particular the subhalo mass of the lens galaxies covers a very broad range. Bias arises simply because the lensing signal depends on these parameters in a non-linear fashion. For subhalo mass, the difference between the peak of the posterior distribution and the input mean value is about 0.1 dex, slightly larger than the 2σ width of the posterior distribution.

One way to suppress the bias is to use narrower mass bins. In our model, the subhalo mass of a satellite depends mainly on its stellar mass although the host halo mass and halo-centric radius also influence somewhat through tidal interactions. Too see the effects of different binning, we split satellites in our fiducial satellite sample into five finer stellar mass bins. The corresponding lensing signal of each of the mass bins is shown in Fig.10, respectively. We then can analyze the host halo and subhalo properties with MCMC by fitting to the lensing signals from the five subsamples

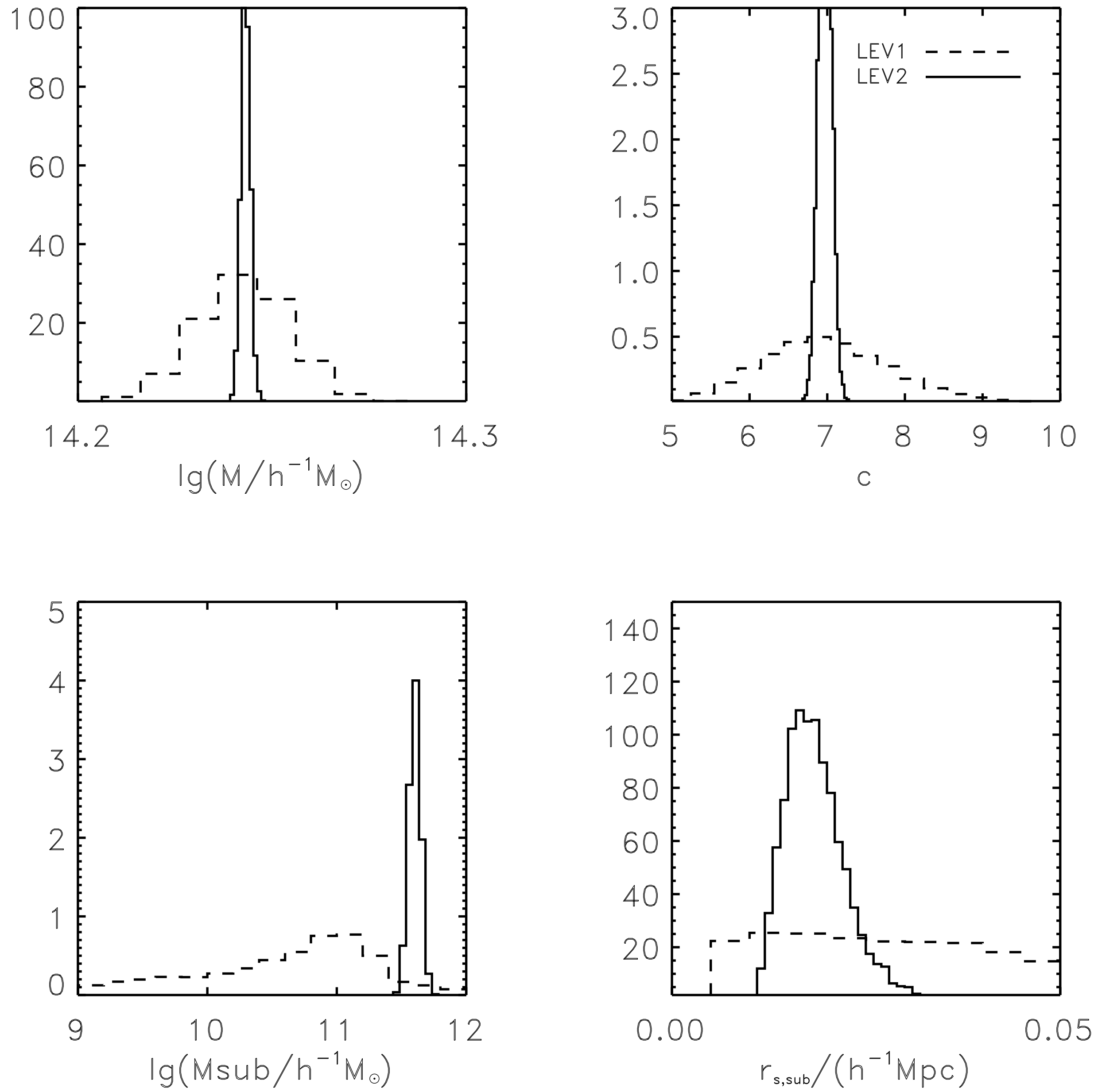

Figure 7. A close comparison between the posterior distributions shown in Figs.5 and 6. The solid histograms are the marginalized distribution of M, c, $M_{\rm sub}$ and $r_{\rm s,sub}$ for LEV2, while the dashed histograms for LEV1 case.

jointly. In principle, we should consider five sets of parameters $(M_{\rm sub}, r_{\rm s,sub}, \rho_{0,\rm sub})$ each for a single bin. We then need to deal with 15 parameters for subhaloes, plus the ones for host haloes. The task would be difficult with the statistics of the expected data. On the the hand, one naturally expects certain relations between different quantities, which can be parameterized with a much smaller number of free parameters. By MCMC fitting to the 'observed' data, we can extract the constraints on these parameters. This approach allows us to control the number of free parameters and at the same time to model the lensing signals better than that from a single broad bin of subhalo mass. As a test, we assume that $M_{\rm sub}/M_*$ depends on the stellar mass M_* according to a power-law,

$$\frac{M_{\rm sub}}{M_*} = a_0 \left(\frac{M_*}{10^{10}{\rm h}^{-1}{\rm M}_\odot}\right)^{a_1} . \qquad (24)$$

Furthermore, we assume that $r_{\rm s,sub}$ and $r_{\rm t}$ depend on subhalo mass through the following parameterizations

$$r_{\rm s,sub} = b_0 \left(\frac{M_{\rm sub}}{10^{12}{\rm h}^{-1}{\rm M}_\odot}\right)^{b_1} , \qquad (25)$$

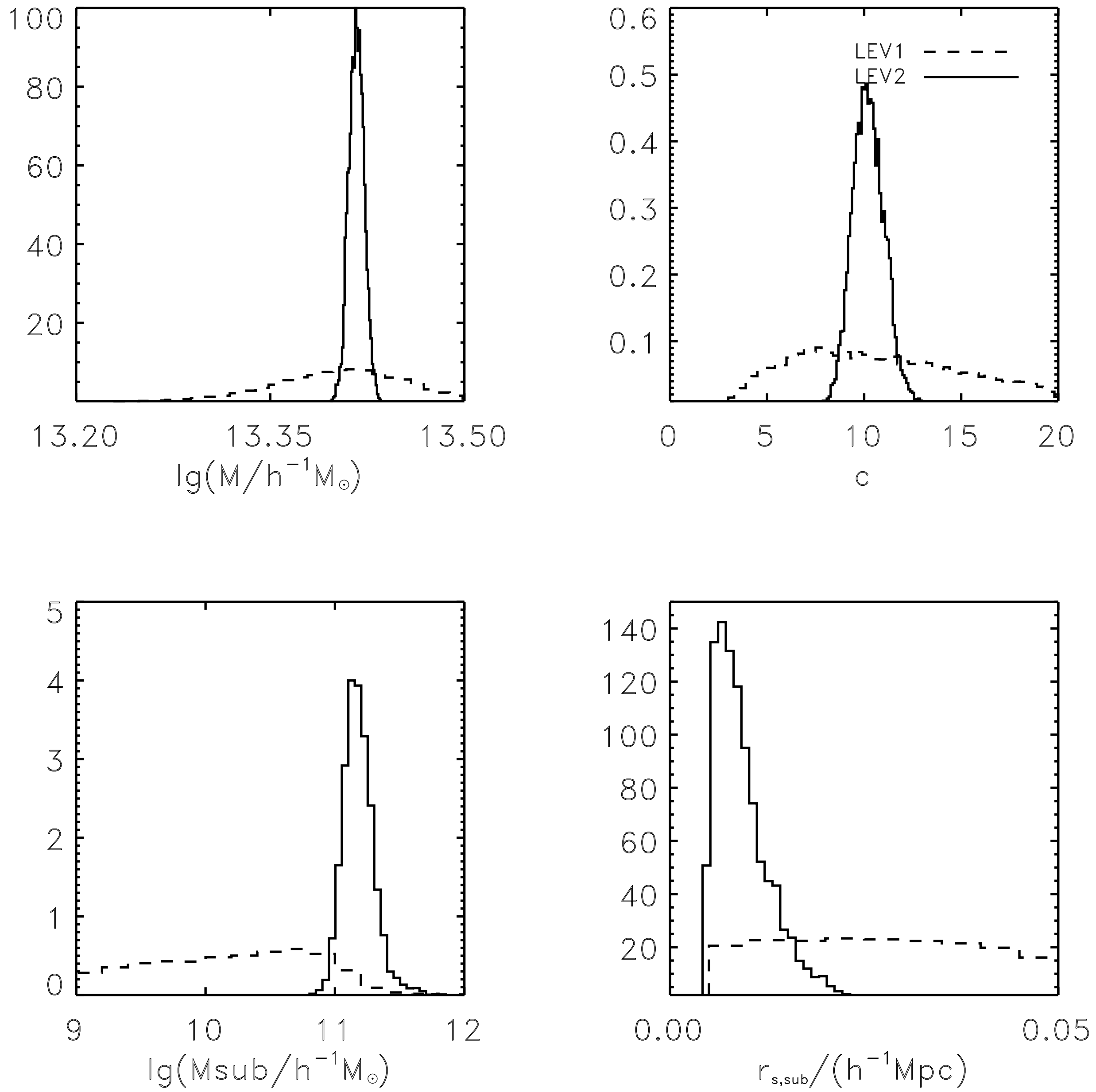

Figure 8. The same as Fig.7, except that here results are shown for satellites in host haloes with masses in the range $[10^{13}, 5\times10^{13}]\mathrm{h}^{-1}\mathrm{M}_\odot$ and with projected halo-centric distance in range $[0.5, 0.6]\mathrm{h}^{-1}\mathrm{Mpc}$.

and

$$r_{\rm t} = c_0 + c_1\, r_{\rm s,sub}\,, \qquad (26)$$

where a_0, a_1, b_0, b_1, c_0 and c_1 are all free parameters. We then fit the mock lensing data from all 5 stellar mass bins simultaneously to derive constraints on these parameters. Fig.11 shows the 68% and 95% confidence range of the marginalized posterior probability distributions for these subhalo parameters. For comparison, the 'true input' values, obtained by directly fitting relations (24), (25), and (26) to the input subhaloes, are marked with the plus symbol in each panel. We can see that the 68% posterior contours enclose the input values, indicating that the bias due to binning can be effectively reduced by dividing lens galaxies into fine bins.

6.2 Contamination from fake group members

So far we have not considered possible contaminations in the group catalog and assumed that all galaxies assigned to a group are true members. In reality, however, some galaxies that are identified as satellites may actually be central galaxies of other (low-mass) haloes along the line of sight. In what

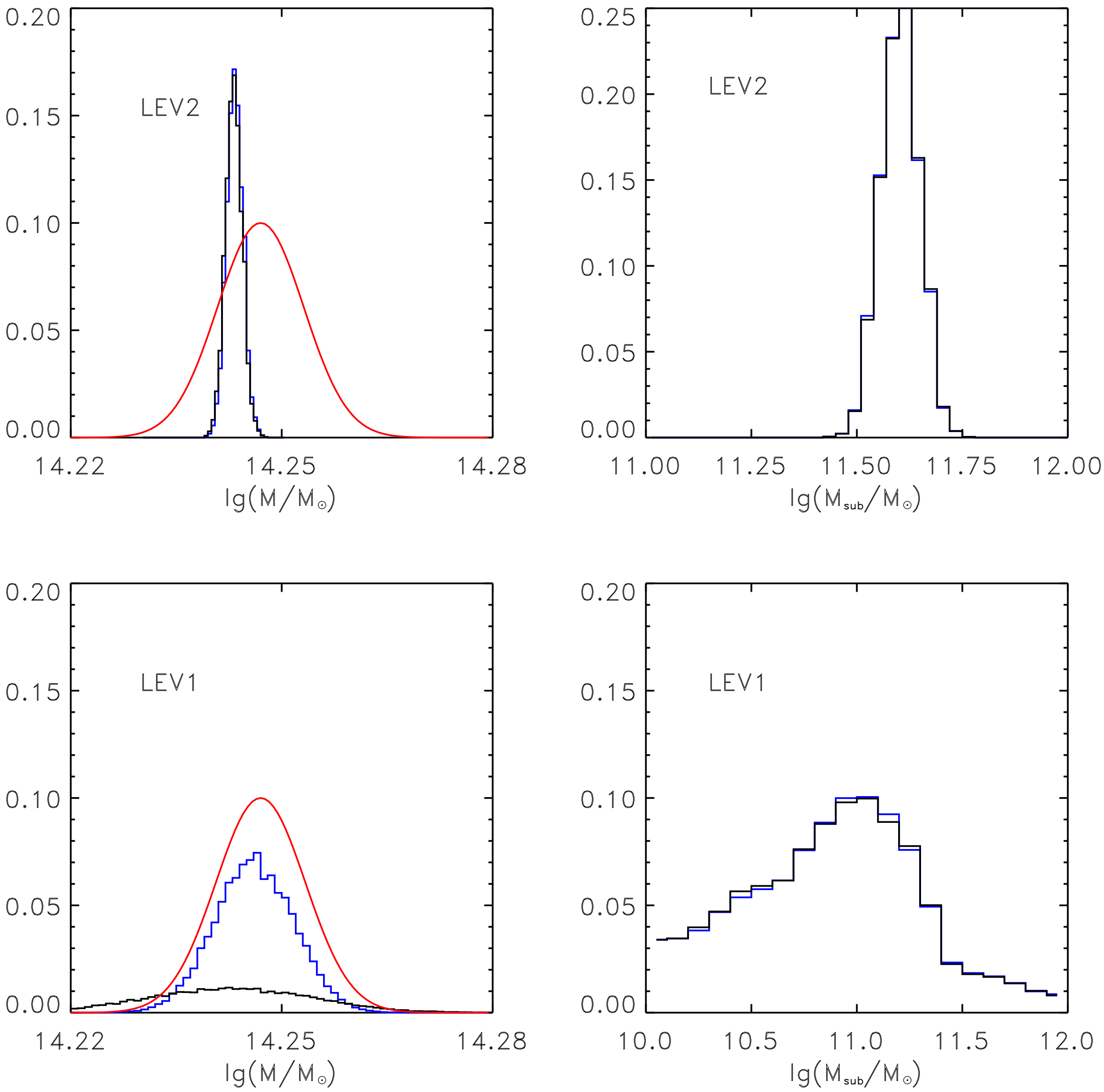

Figure 9. The figure shows the effect of priors of host halo mass on parameter constraining.The black(blue) histogram represents the marginalized posterior distribution of M(left column) and subhalo mass(right column) with flat prior(lognormal prior). The upper panels show the results for LEV2 case and the lower panels show the results for LEV1 case. In the left panels, the red solid lines show the prior distribution of halo mass. We scale the amplitude of prior distribution, so that it can be shown in the same panel with posterior distribution.

follows, we refer to such galaxies as interlopers. For galaxies of the same luminosity, central galaxies produce much stronger lensing signals than that of satellites. Hence, even an interloper fraction of 10% can introduce significant errors in the inferred subhalo parameters.

To estimate the impact of interlopers, we make use of the SDSS mock group catalog provided by Yang et al. (2007). This mock catalog is constructed by running the halo-based group finder of Yang et al. (2005) on a mock galaxy redshift survey (MGRS) built by populating dark matter haloes with galaxies according to the conditional luminosity function(CLF; van den Bosch et al. 2007). The CLF, which describes the luminosity distribution for galaxies in haloes of a given mass, is constrained using the clustering and abundances of galaxies in the SDSS. As the result, the luminosity function and clustering properties of the MGRS accurately matches those of the SDSS. . The MGRS also takes into account of real observational conditions by mimicking the sky coverage and completeness trend of the SDSS survey (see Yang et al. (2007) for the detail). For such a mock group catalog, we not only know the group to which a galaxy is assigned, but also the dark matter halo to which the galaxy truly belongs. Thus, it is particular suitable to examine the potential bias that arises due to interlopers.

From the SDSS mock group catalog, we select satellites in groups with assigned host mass from the group finder in

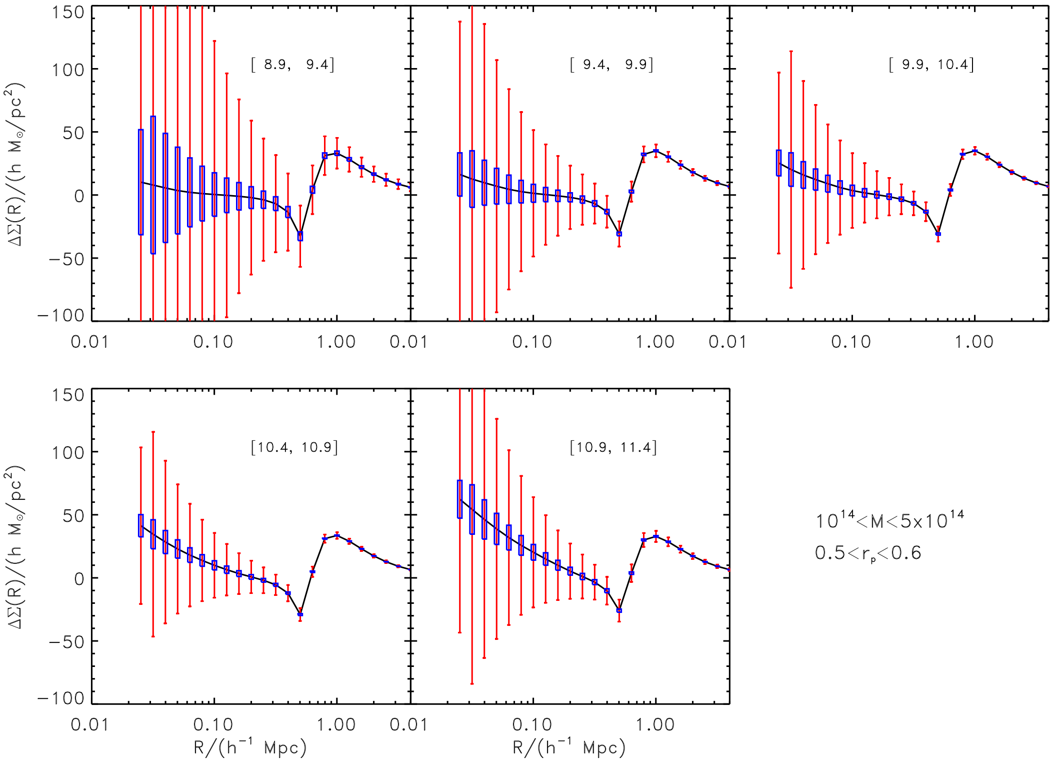

Figure 10. The lensing signal around satellite galaxies in different stellar mass range. All satellite galaxies are selected from groups of $[10^{14}, 5 \times 10^{14}]\mathrm{h}^{-1}\mathrm{M}_{\odot}$, and with projected halo centric distance of $[0.5, 0.6]\mathrm{h}^{-1}\mathrm{Mpc}$. Each subplot shows lensing signal of satellites in certain stellar mass bin. We mark the $\log(M*/\mathrm{h}^{-1}\mathrm{M}_{\odot})$ range for each subsample in subplots. The red errorbars show the noise estimation of LEV1 (SDSS like survey), while the blue rectangles show the LEV2 noise (LSST like survey).

the range of $[10^{14}, 2 \times 10^{14}]\mathrm{h}^{-1}\mathrm{M}_{\odot}$ and with the projected halo-centric distance of $[0.5, 0.6]\mathrm{h}^{-1}\mathrm{Mpc}$. We use the model described in Section 3 to generate mock galaxy-galaxy lensing data. To isolate the errors due to interlopers, we fix the subhalo mass to be $10^{11.7}\mathrm{h}^{-1}\mathrm{M}_{\odot}$ in calculating the fiducial data, which is similar to the mean subhalo mass of SDSSGC satellites used in previous sections. We find that about 10% of the selected satellite galaxies are actually centrals of other host haloes (i.e., are interlopers). We then assign each of them a NFW profile according to their host halo mass. The resulting lensing signals are shown in Fig.12, where the solid line is the excess surface density profile of the true satellite galaxies, and the dashed line shows the signal due to the interlopers. As can be seen, the interlopers contribute about 15% of the total signal in the inner part, which in turn can lead to large bias in the model fitting. Fig.13 shows the bias in subhalo mass introduced by these interlopers. We fit two sets of lensing signals separately. The first set contains contributions from both true satellites and interlopers. This is referred to as the 'mixed' signal. The second set contains only true satellite galaxies, and is referred to as the 'true' signal. The solid line is the constraint from the 'true' signals and the dashed line is from the 'mixed' signals. The vertical line indicates the input subhalo mass. We can see that the subhalo mass inferred from the 'mixed' signal is biased high by $\sim 50\%$ compared to that inferred from the 'true' signal. The latter result is very consistent with the input value.

The above analyses shows that it is important to carefully consider the impact of interlopers in the group catalog. Unfortunately, it is virtually impossible to completely eliminate interlopers. In fact, the halo based group finder of Yang et al. (2005) has been optimized to minimize the impact of interlopers, among some other constraints. Rather than trying to reduce (or eliminate) interlopers, one may also try to account for them in the modeling. Using empirical relations between the luminosity/stellar mass of central galaxies and their host halo mass (see e.g. Yang et al. 2007) it is fairly straightforward to fit for subhalo mass and interloper fraction simultaneously. As a test, we assume that each galaxy in the selected sample has the same possibility $P_{\rm con}$ to be a central galaxy. We use the relation between the central galaxy luminosity and its host halo mass from our MGRS to assign a halo mass to a central galaxy. The total signal is then modeled as,

$$\Delta\Sigma(R) = \Delta\Sigma_{\rm sat}(R)(1 - P_{\rm con}) + \Delta\Sigma_{\rm cen}(R)P_{\rm con} \, , \qquad (27)$$

where $\Delta\Sigma_{\rm sat}$ is the lensing signal calculated by assuming no contamination, and $\Delta\Sigma_{\rm cen}$ is the lensing signal calculated by assuming that all satellites selected are actually central galaxies of other haloes. The fitting result is shown in Fig.14. Although the posterior distribution shows degeneracy between $P_{\rm con}$ and $M_{\rm sub}$, the bias due to contamination is now suppressed. If the MGRS is sufficiently realistic, we should in principle be able to obtain some estimates for the interloper fractions, which can then be used as a prior in the MCMC fitting. This should allow for tight and unbiased constraints on the subhalo mass.

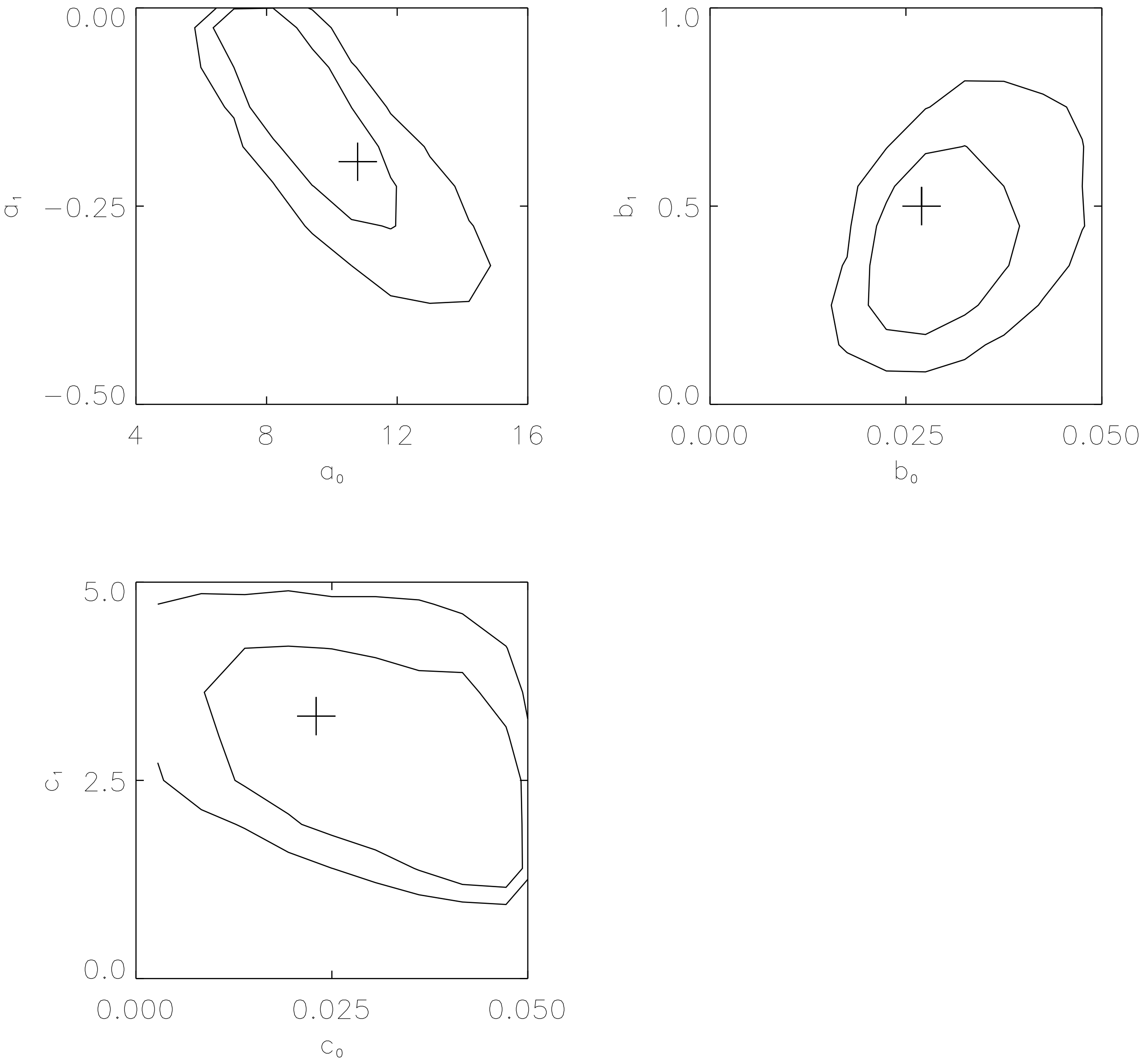

Figure 11. Fitting results for lensing signal in Fig.10. Contours show 68% and 95% confidence range of the marginalized posterior probability distribution. The plus marks show the true inputs value.

7 SUMMARY

In this paper, we have investigated the feasibility of constraining the masses and density profiles of dark matter subhaloes associated with satellite galaxies using galaxy-galaxy lensing. With the use of a group catalog constructed from a large redshift survey, such as the SDSS, we can effectively distinguish central and satellite galaxies. Therefore we can select satellite galaxies according to their host halo mass, halo-centric distance and stellar mass. By stacking the galaxy-galaxy lensing signal of satellite galaxies with similar properties, we can then study both the host halo and subhalo density profiles. In this paper, we have used the SDSS group catalog constructed by Yang et al. (2007) to predict the galaxy-galaxy lensing signal for satellite galaxies residing in different host haloes and located at different halo-centric distances. To examine to what extent such data can be used to infer the properties of host and sub-halo, we have considered two different noise levels, LEV1 and LEV2, that correspond to the levels of measurement noise expected from a current generation galaxy survey, such as SDSS, and from a next generation galaxy survey, such as LSST, respec-

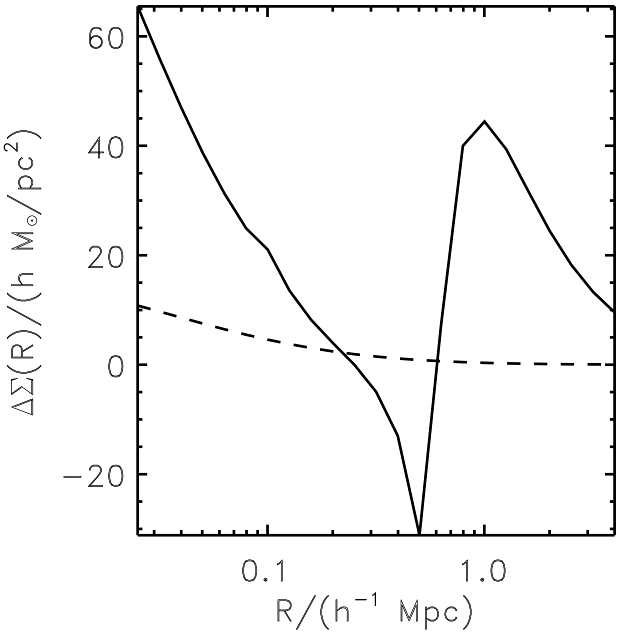

Figure 12. The figure shows the lensing signal of galaxies in mock SDSS group catalog. The galaxies are selected from haloes of $[10^{14}, 2 \times 10^{14}]\mathrm{h}^{-1}\mathrm{M}_{\odot}$ with halo-centric radius of $[0.5, 0.6]\mathrm{h}^{-1}\mathrm{Mpc}$. The signal from true satellites is represented by solid line and that from fake members by dashed line.

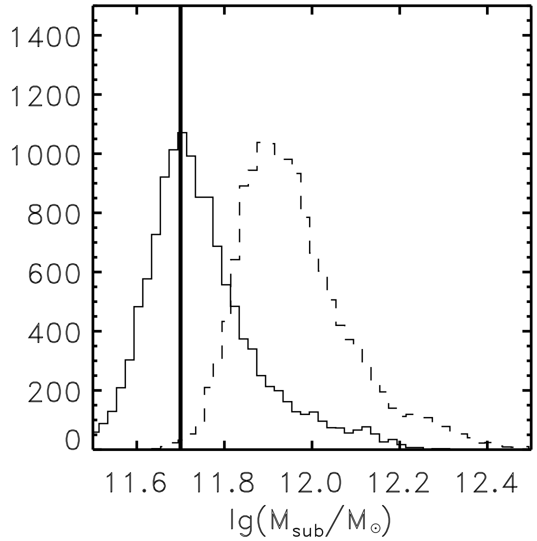

Figure 13. The 1-d constraint on the subhalo mass. The dashed and solid lines are for the results derived from fitting to the 'mixed' and 'ture' signals of satellites, respectively. The vertical line indicates the input value of the subhalo mass.

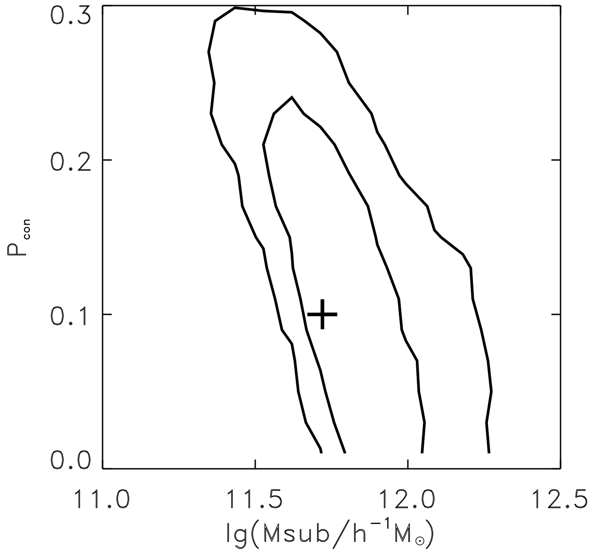

Figure 14. Fitting to the mixed lensing signal of mock catalog. The contour shows 2d posterior distribution of $M_{\rm sub}$ and $P_{\rm con}$. The plus mark represents input value.

tively. Using the MCMC method, we investigated how well LEV1 and LEV2-type data can constrain the mass and density profile for subhaloes and host haloes simultaneously. For satellite galaxies in massive groups, with host halo masses in the range of $[10^{14}, 5 \times 10^{14}]\mathrm{h}^{-1}\mathrm{M}_{\odot}$, the density profile of the host halo can be well constrained for both LEV1 and LEV2 noise levels. However, the data quality that is achievable with current LEV1-type surveys is insufficient to put any meaningful constraints on the subhalo properties. In the case of a LEV2-type survey, on the other hand, the galaxy-galaxy lensing data is predicted to be of sufficient quality that one can put tight constraints on the average subhalo mass, with a 1σ confidence of about 0.2 dex. Even the amplitude and characteristic scale of the subhalo density profiles can be constrained, albeit with still relatively large uncertainties. We also demonstrate that, with LEV2-type surveys, it is even possible to probe subhaloes in group-sized host haloes with masses as low as $10^{13}\mathrm{h}^{-1}\mathrm{M}_{\odot}$.

We also discussed some potential systematics that result in biased estimates. One of these arises from the fact that one stacks the signal from satellite galaxies that span a significant range in properties of host halo and subhalo. Since the lensing signal does not scale linearly with model parameters, the best fit of the mean value of the parameters can be biased relative to the underlying values of the stacked sample. We have shown that such bias can be reduced by dividing the satellite sample into finer stellar mass bins and using parameterized forms for the scaling relations between satellite and subhalo properties. Another bias arises from the presence of interlopers in the group catalog (i.e., from galaxies that have erroneously been assigned to a group due to projection effects). This implies that some of the galaxies identified as satellites in the group catalog are actually centrals of other (typically low-mass) haloes. Our test using a mock SDSS group catalog shows that about 10% of the satellites are such interlopers. Such a contamination can bias the inferred subhalo mass high by $\sim 50\%$. To overcome the bias effect, we propose to include the contamination fraction as a free parameter in the model fitting. Our test shows that the bias in the subhalo mass due to the contamination can be effectively removed at the expense of enlarged uncertainties. This uncertainty, in turn, can be reduced by using priors on the interloper fractions which can be obtained from realistic mock galaxy redshift surveys. We conclude that measurement of galaxy-galaxy lensing around satellite galaxies with future surveys such as LSST holds great promise for constraining the properties of dark matter substructure.

ACKNOWLEDGMENTS

LR is supported by China Postdoctoral Science Foundation, Grant NO. 2011M500395. Part of the computation was carried out on the SGI Altix 330 system at the Department of Astronomy, Peking University. ZHF is supported in part by the NSFC of China under grants 11033005 and 11173001

REFERENCES

Abazajian K. N., Adelman-McCarthy J. K., Agüeros M. A., Allam S. S., Allende Prieto C., An D., Anderson K. S. J., 2009, ApJS, 182, 543

Bartelmann M., 1996, A&A, 313, 697

Bell E. F., McIntosh D. H., Katz N., Weinberg M. D., 2003, ApJS, 149, 289

Bernstein G. M., Jarvis M., 2002, AJ, 123, 583

Binney J., Tremaine S., 1987, Galactic dynamics

Bolton A. S., Treu T., Koopmans L. V. E., Gavazzi R., Moustakas L. A., Burles S., Schlegel D. J., Wayth R., 2008, ApJ, 684, 248

Brainerd T. G., Blandford R. D., Smail I., 1996, ApJ, 466, 623

Bullock J. S., Kolatt T. S., Sigad Y., Somerville R. S., Kravtsov A. V., Klypin A. A., Primack J. R., Dekel A., 2001, MNRAS, 321, 559

Cacciato M., van den Bosch F. C., More S., Li R., Mo H. J., Yang X., 2009, MNRAS, 394, 929

Chib S., Greenberg E., 1995, American Statistician, 49, 327

Diemand J., Kuhlen M., Madau P., 2007, ApJ, 657, 262

Dolag K., Bartelmann M., Perrotta F., Baccigalupi C., Moscardini L., Meneghetti M., Tormen G., 2004, A&A, 416, 853

Eke V. R., Navarro J. F., Steinmetz M., 2001, ApJ, 554, 114

Gao L., White S. D. M., Jenkins A., Stoehr F., Springel V., 2004, MNRAS, 355, 819

Gill S. P. D., Knebe A., Gibson B. K., 2004, MNRAS, 351, 399

Giocoli C., Tormen G., Sheth R. K., van den Bosch F. C., 2010, MNRAS, 404, 502

Giocoli C., Tormen G., van den Bosch F. C., 2008, MNRAS, 386, 2135

Hamana T., Takada M., Yoshida N., 2004, MNRAS, 350, 893

Hastings W. K., 1970, Biometrika, 57, 97

Hayashi E., Navarro J. F., Taylor J. E., Stadel J., Quinn T., 2003, ApJ, 584, 541

Hoekstra H., 2004, MNRAS, 347, 1337

Hoekstra H., Franx M., Kuijken K., Carlberg R. G., Yee H. K. C., 2003, MNRAS, 340, 609

Hu W., Kravtsov A. V., 2003, ApJ, 584, 702

Hudson M. J., Gwyn S. D. J., Dahle H., Kaiser N., 1998, ApJ, 503, 531

Jing Y. P., 2000, ApJ, 535, 30

Johnston D. E., Sheldon E. S., Tasitsiomi A., Frieman J. A., Wechsler R. H., McKay T. A., 2007, ApJ, 656, 27

Kochanek C. S., Dalal N., 2004, ApJ, 610, 69

Komatsu E., Smith K. M., Dunkley J., Bennett C. L., Gold B., Hinshaw G., Jarosik N., Larson D., 2010, ArXiv e-prints

Koopmans L. V. E., 2005, MNRAS, 363, 1136

Lewis A., Bridle S., 2002, PhRevD, 66, 103511

Li R., Mo H. J., Fan Z., Cacciato M., van den Bosch F. C., Yang X., More S., 2009, MNRAS, 394, 1016

Limousin M., Kneib J. P., Bardeau S., Natarajan P., Czoske O., Smail I., Ebeling H., Smith G. P., 2007, A&A, 461, 881

Macciò A. V., Dutton A. A., van den Bosch F. C., Moore B., Potter D., Stadel J., 2007, MNRAS, 378, 55

Macciò A. V., Miranda M., 2006, MNRAS, 368, 599

Mandelbaum R., Hirata C. M., Seljak U., Guzik J., Padmanabhan N., Blake C., Blanton M. R., Lupton R., Brinkmann J., 2005, MNRAS, 361, 1287

Mandelbaum R., Seljak U., Hirata C. M., 2008, JCAP, 8, 6

Mandelbaum R., Seljak U., Kauffmann G., Hirata C. M., Brinkmann J., 2006, MNRAS, 368, 715

Mao S., Jing Y., Ostriker J. P., Weller J., 2004, ApJL, 604, L5

Mao S., Schneider P., 1998, MNRAS, 295, 587

McKay T. A., Sheldon E. S., Racusin J., Fischer P., Seljak U., Stebbins A., Johnston D., Frieman J. A. a., 2001, ArXiv Astrophysics e-prints

Metcalf R. B., Madau P., 2001, ApJ, 563, 9

Metropolis N., Rosenbluth A., Rosenbluth M., Teller A., H. T., 1953, Journal of Chemical Physics, 21, 1087

Metropolis N., Ulam S., 1949, J. Amer.Statist.Assoc, 44, 335

Natarajan P., De Lucia G., Springel V., 2007, MNRAS, 376, 180

Natarajan P., Kneib J.-P., Smail I., Treu T., Ellis R., Moran S., Limousin M., Czoske O., 2009, ApJ, 693, 970

Navarro J. F., Frenk C. S., White S. D. M., 1997, ApJ, 490, 493

Oguri M., Lee J., 2004, MNRAS, 355, 120

Pastor Mira E., Hilbert S., Hartlap J., Schneider P., 2011, A&A, 531, A169

Sheldon E. S., Johnston D. E., Scranton R., Koester B. P., Mc Kay T. A., Oyaizu H., Cunha C., Lima M., Lin H., Frieman J. A., Wechsler R. H., Annis J., Mandelbaum R., Bahcall N. A., Fukugita M., 2009, ApJ, 703, 2217

Springel V., Wang J., Vogelsberger M., Ludlow A., Jenkins A., Helmi A., Navarro J. F., Frenk C. S., 2008, MNRAS, 391, 1685

Taylor J. E., Babul A., 2004, MNRAS, 348, 811

Tormen G., Diaferio A., Syer D., 1998, MNRAS, 299, 728

van den Bosch F. C., Tormen G., Giocoli C., 2005, MNRAS, 359, 1029
van den Bosch F. C., Yang X., Mo H. J., Weinmann S. M., Macciò A. V., More S., Cacciato M., Skibba R., Kang X., 2007, MNRAS, 376, 841
Vegetti S., Koopmans L. V. E., 2009a, MNRAS, 392, 945
Vegetti S., Koopmans L. V. E., 2009b, MNRAS, 400, 1583
Vegetti S., Koopmans L. V. E., Bolton A., Treu T., Gavazzi R., 2010, MNRAS, 408, 1969
Vegetti S., Lagattuta D. J., McKean J. P., Auger M. W., Fassnacht C. D., Koopmans L. V. E., 2012, Nature, 481, 341
Wechsler R. H., Bullock J. S., Primack J. R., Kravtsov A. V., Dekel A., 2002, ApJ, 568, 52
White S. D. M., Frenk C. S., 1991, ApJ, 379, 52
White S. D. M., Rees M. J., 1978, MNRAS, 183, 341
Wright C. O., Brainerd T. G., 2000, ApJ, 534, 34
Xu D. D., Mao S., Wang J., Springel V., Gao L., White S. D. M., Frenk C. S., Jenkins A., Li G., Navarro J. F., 2009, MNRAS, 398, 1235
Yang X., Mo H. J., van den Bosch F. C., 2008, ApJ, 676, 248
Yang X., Mo H. J., van den Bosch F. C., Jing Y. P., 2005, MNRAS, 356, 1293
Yang X., Mo H. J., van den Bosch F. C., Jing Y. P., Weinmann S. M., Meneghetti M., 2006, MNRAS, 373, 1159
Yang X., Mo H. J., van den Bosch F. C., Pasquali A., Li C., Barden M., 2007, ApJ, 671, 153
Zentner A. R., Bullock J. S., 2003, ApJ, 598, 49
Zhao D. H., Jing Y. P., Mo H. J., Börner G., 2003, ApJL, 597, L9
Zhao D. H., Jing Y. P., Mo H. J., Börner G., 2009, ApJ, 707, 354